Journal of Quantitative Spectroscopy & Radiative Transfer 331 (2025) 109272

Contents lists available at ScienceDirect

Journal of Quantitative Spectroscopy and Radiative Transfer

journal homepage: www.elsevier.com/locate/jqsrt

Dielectronic satellite spectra from hollow He- and Li-like ion states in fluorine

A.S. Safronova *, A. Stafford, U.I. Safronova [1]

University of Nevada, Reno, NV 89557, USA

ARTICLE INFO

Keywords:
Plasma spectroscopy
Hollow ions
K-shell dielectronic satellite spectra
He- and Li-like Fluorine ions

ABSTRACT

About two decades ago, very unusual highly-resolved x-ray spectra were observed using a femtosecond laser-produced plasma that included a new type of satellite lines identified as being emitted from the autoionizing states of hollow ions (such as, for example, exotic KK hollow ions with the empty K shell). Though atomic structure calculations were able to predict the locations of such newly observed spectral features with reasonable precision, the relatively high intensity of these so-called hypersatellite lines, produced mainly in high-power laser plasmas, is far from being understood. The analysis of previous experiments with Teflon on the Leopard laser performed under different conditions related to laser pulse and contrast revealed the existence of KK hollow fluorine ions and motivated systematic theoretical studies of dielectronic satellite spectra from hollow ion states starting with He- and Li-like fluorine ions presented in this paper.

1. Introduction

One of the greatest advances in plasma spectroscopy since the late 1960s was the discovery and use of satellite lines to understand the atomic processes and parameters in both astrophysical and laboratory plasmas by Gabriel et al. [1,2]. Such spectral lines appearing near the resonance lines of the highly ionized systems were found to originate from the autoionizing doubly-excited states and to represent a very useful diagnostic tool of high temperature plasmas (see, for example, Ref. [3], for astrophysical applications). Theoretically, the wavelengths, radiative transition probabilities, autoionization rates, and intensity factors for dielectronic satellite transitions from doubly-excited states in Helium (He)–like and Lithium (Li)-like ions ($2p2l \rightarrow 1s2l$ and $1s2p2l \rightarrow 1s^2 2l$, respectively) were calculated for atomic numbers $Z = 4$–34 with high precision by Vainstein and Safronova using the MZ code based on the quasi-relativistic many-body perturbation theory (MBPT) Z-expansion method [4]. This method (which includes relativistic corrections taken into account within the framework of the Breit operator) was explained in detail by Safronova and Urnov in Refs. [5,6]. It was applied to dielectronic satellite spectra for highly charged Li- to O-like Mg and Fe ions in hot dense plasmas [7]. Recently, similar calculations but with the modified MZ code, which accounted for the first order corrections in powers of 1/Z (corresponding to the screening effects in calculations of autoionization rates) have been carried out [8]. Using the perturbation theory approach similar to [4–6], Safronova and Senashenko studied radiative and autoionization decay rates for the exotic atomic systems with two K-shell vacancies [9,10], later named "KK hollow states". In particular, autoionizing triply-excited states have been theoretically studied. The MBPT method was used in [9] to calculate energies and rates for the radiative and autoionization decays of the Li-like ions with two K-shell vacancies: $2s^2 2p$, $2s2p^2$, and $2p^3$. Wavelengths and transitions rates were calculated for the $[2s^2 2p + 2p^3] \rightarrow [1s2s^2 + 1s2p^2]$ and $2s2p^2 \rightarrow 1s2s2p$ transitions in Fe^{23+} and Ni^{25+} ions [10]. Experimental evidence for the possible formation of such autoionizing triply-excited states was obtained in the beam-foil experiments, where lines were revealed in the electron spectrum observed after the passage of 300 keV Li^+ ions through thin carbon films, and their appearance was attributed to decay of autoionizing triply-excited states of Li atoms by Bruch et al. [11]. A comprehensive study of triply-excited states of the Li isoelectronic sequence was presented almost two decades later in [12]. Important atomic characteristics such as radiative and autoionization decay rates were computed and analyzed and the results were compared with available theoretical and experimental data for Li I and Be II. All atomic characteristics were calculated for a wide range of atomic numbers $Z = 3$–54, which allowed to investigate Z-dependencies of such characteristics in detail [12].

* Corresponding author at: 1664 N. Virginia St., Department of Physics MS 220, University of Nevada, Reno, NV 89557.
E-mail address: alla@physics.unr.edu (A.S. Safronova).
[1] Deceased author.

https://doi.org/10.1016/j.jqsrt.2024.109272
Received 17 May 2024; Received in revised form 12 November 2024; Accepted 13 November 2024
Available online 16 November 2024

About two decades ago, very unusual highly-resolved x-ray spectra were observed using a femtosecond laser-produced plasma that included a new type of satellite lines identified as being emitted from the autoionizing states of hollow ions (such as, for example, exotic KK hollow ions with the empty K shell). Specifically, high-resolved x-ray spectra of hollow Mg, Al, and Si ions in a femtosecond laser-produced solid plasma were obtained by Faenov et al. [13]. Experiments were carried out both on TRIDENT (at the Los Alamos National Laboratory) and in the Center for Ultrafast Optical Science (at the University of Michigan) laser facilities. X-ray plasma emission was recorded with the high-resolved spectrometer with a spherical bent mica crystal. The atomic spectra calculations using HULLAC and SUPERSTRUCTURE codes showed that the spectral regions under study were covered by numerous lines originated from transitions in many-electron systems with KK hollow states in Li- and Be-like ions [13]. The review of the spectra of hollow ions in laser plasmas [14] discusses the observation of the spectra of hollow ions in an ultradense laser plasma and considers the types of such ions and how they are created. Considerable opportunities of hollow ion spectra-based diagnostic techniques are emphasized [14]. For example, diagnostics of the early stage of the heating of clusters by a femtosecond laser pulse from the spectra of hollow ions was proposed and discussed in [15]. It has been shown that the spectra of hollow ions are the most informative in the first moments of the heating of a cluster, whereas the diagnostics of the late stages can be performed using the conventional lines of multicharged ions [15].

Charge-exchange-induced formation of hollow atoms in high-intensity laser-produced plasmas was presented by Rosmej et al. [16]. Authors underlined that for the first time registration of high-resolution soft x-ray emission of hollow-atom dielectronic satellite spectra of highly charged nitrogen were performed. Double-electron charge-exchange processes from excited states were proposed in [16] as a mechanism of formation of autoionizing levels $nln'l'$ (with n = 3–8, n'= 5–8 and l, l' = 0–7) in high-intensity laser-produced plasmas, when field-ionized ions penetrate into the residual gas. The formation of hollow ions in dense Z-pinch and laser- produced plasmas was investigated using high-resolution x-ray spectroscopy and atomic data calculations by Rosmej et al. [17]. Dense plasma effects were found to result in highly populated excited states which open up excitation channels not accessible in low-density plasma sources. Experimental argon spectra from a Mega-Ampere Z-pinch were interpreted in [17] as the $2s^n2p^m \rightarrow 1s2s^n2^{m-1}$ transitions in hollow Ar ions. Theoretical wavelengths of the transitions $2l2l'2l'' \rightarrow 1s2l2l'$ were compared with experimental ones in hollow Ar ions spectra [17]. More recently, Rosmej et al. studied exotic x-ray emission from dense matter which was identified as the complex high intensity satellite emission from autoionizing states of highly charged ions and have demonstrated that charge exchange of intermixing inhomogenous plasmas as well as collisions driven by suprathermal electrons are possible mechanisms to populate hollow ions to observable levels in dense plasmas, particularly in high current Z-pinch plasmas and high intensity field-ionized laser produced plasmas [18].

In high-spectral resolution experiments at the Vulcan Petawatt laser facility, strong x-ray radiation of KK hollow atoms from thin Al foils was observed by Colgan et al. [19] at pulse intensities of 3×10^{20} W/cm^2. The observations of spectra from these exotic states of matter were supported by detailed kinetics calculations. Hansen et al. [20] underlined that x-ray emission from hollow ions offers new diagnostic opportunities for dense, strongly coupled plasma. The extended modeling of the x-ray emission spectrum reported by Colgan et al. [19] was presented in [20]. The first observation of high-n hollow ions produced in Si targets through pumping by ultra-intense x-ray radiation in experiments performed also at the Vulcan Petawatt laser facility was reported in [21].

Atomic physics of relativistic high contrast laser-produced plasmas has been studied in experiments on Leopard laser facility at UNR by Safronova et al. [22], which were performed under different experimental conditions related to laser pulse and contrast. In particular, the duration of the laser pulse was 350 fs or 0.8 ns and the contrast varied from high (10^{-7}) to moderate (10^{-5}). The thin laser targets (from 4 to 750 μm) made of a broad range of materials (from Teflon to iron and molybdenum to tungsten and gold) were utilized. Using a high-precision x-ray spectrometer with resolution R~3000 and a survey x-ray spectrometer, the unique spectral features were observed that are illustrated in [22]. In addition to l-shell Fe and Cu spectra that were studied for electron beam diagnostics, K-shell Mg features with dielectronic satellites from high-Rydberg states and the new K-shell F features with dielectronic satellites including exotic transitions from hollow ions were highlighted. Specifically, K-shell Mg spectra with complex satellite features which were collected from experiments comprised of three different conditions related to laser pulse and contrast were studied by Stafford et al. [23]. They included DS lines that were identified and modeled as transitions from autoionizing $2lnl'$ states in He-like Mg and from autoionizing $1s3lnl'$ states in Li-like Mg and $1s3l3l'3l''$ states in Be-like Mg ions. The analysis of previous experiments with Teflon on the Leopard laser performed under different conditions related to laser pulse and contrast revealed the existence of KK hollow fluorine ions [22] and motivated theoretical studies of dielectronic satellite spectra from hollow ion states in He- and Li-like F ions presented in this paper.

In the present paper, we report on the theoretical study of dielectronic satellite spectra from hollow He- and Li-like states in fluorine (F). In particular, Section 2 provides basic formulae and illustrations of dielectronic satellite spectra from autoionizing doubly-excited states in He- and Li-like F ions. Section 3 presents atomic data and dielectronic satellite spectra from hollow triply-excited states in Li-like F. Section 4 highlights the applications of Li-like F results from Section 3 to high-density plasmas, and Section 5 discusses the accuracy of atomic data for hollow Li-like F ions and includes conclusions.

2. Basic formulae and dielectronic satellite lines from autoionizing doubly-excited states in He- and Li-like fluorine

Dielectronic Recombination (DR) process was studied in detail by many authors and can be explained using the simplest case of He-like fluorine (F) ion. It involves the capture of an electron by a H-like ion to an autoionizing level of the resulting He-like ion followed by radiative decay to a singly-excited bound level:

$$\begin{array}{l} F^{8+}(1s) + e \rightarrow F^{7+**}(2ln'l') \rightarrow F^{7+*}(1sn_1l_1) + h\nu \\ \qquad\qquad\qquad\quad \downarrow \\ \qquad\qquad\qquad\quad F^{8+}(1s) + e \end{array} \tag{1}$$

The ground level of F^{8+}, $1s$, is the initial level. The $2pn'l'$ levels are taken into account as autoionizing intermediate levels. During the DR process, a dielectronic satellite (DS) line is emitted, $h\nu$, when the electron jumps from an autoionizing doubly-excited state to a singly-excited bound state $1sn_1l_1$. Radiative transitions from the doubly-excited $nln'l'$ states to the $1sn_1l_1$ states give rise to satellite lines to the np-1 s transitions in H-like F.

Fig. 1 displays energy level diagram of H-like, He-like, and Li-like F ions and illustrates resonance lines, associated commonly used satellite transitions, and hypersatellites (i.e., transitions from KK hollow ions with the empty 1 s shell) studied in this paper. It resembles the schematic diagram of observed transitions in H- to Li-like Si ions, including high-n hollow-ion emission, shown in [21]. The most diagnostically important resonance lines of K-shell F ions are H-like lines Lyα ($2p \rightarrow 1s$) at λ=14.982 Å and Lyβ ($3p \rightarrow 1s$) at λ=12.643 Å; and He-like lines Heα ($1s2p\ ^1P_1 \rightarrow 1s^2\ ^1S_0$) at λ=16.809 Å, Heβ ($1s3p\ ^1P_1 \rightarrow 1s^2\ ^1S_0$) at λ=14.459 Å, and Heγ ($1s4p\ ^1P_1 \rightarrow 1s^2\ ^1S_0$) at λ=13.782 Å (see Fig. 1). DS lines of He- and Li-like F ions shown in Fig. 1 will be discussed later in the paper. However, the energy level diagram in Fig. 1 shows that additional decay channels for the high-Rydberg autoionizing states can occur. For hollow He-like ions, the $2ln'l'$ states have autoionization decays to $1s$ as shown in Eq. (1) but the $3l3l'$ states have strong autoionization decays to $2l$, which can be larger than to $1s$ by a few orders of magnitude. For

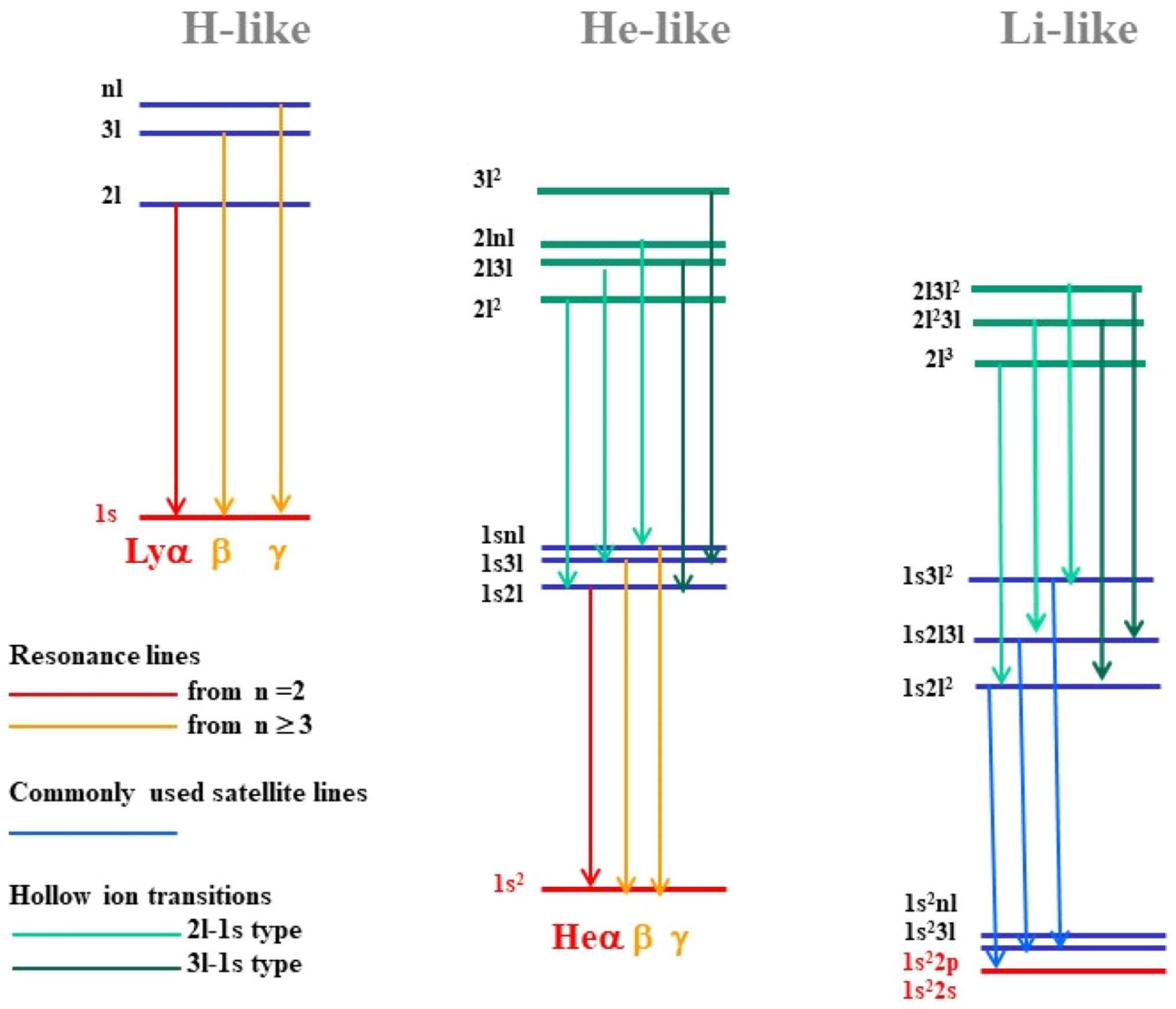

Fig. 1. Energy level diagram of H-, He-, and Li-like F ions, showing resonance lines, associated commonly used satellite transitions, and hollow ion transitions. Notations of configurations are as follows: $nl^2 = nl'nl''$ (n = 2 and 3), and $2l^3 = 2l'2l''2l'''$. Note that the hollow Li-like F states with $n > 3$ are not included in this diagram.

example, the values of A_a for $3d^2\ J = 4$ states can reach $10^{15}\ s^{-1}$ which is 4 orders of magnitude higher than that to 1*s*.

For the DS lines, the modified intensity factor $\widetilde{Q}_d$ is defined as (see, for example, [4,7,23–24]):

$$\widetilde{Q}_d(i,\ j) = \frac{g(i)A_r(i,\ j)A_a(i)}{A_a(i) + \sum_k A_r(i,\ k)} \tag{2}$$

Here *i* is the autoionizing (upper) state, *j* denotes a bound or doubly-excited (lower) state. The statistical weight of the autoionizing state is *g* (*i*), $A_r(i, j)$ is the radiative transition rate from *i* to *j*, and $A_a(i)$ is the total autoionization decay rate summed over all possible radiationless decays from *i*.

Assuming a Maxwellian distribution for free electrons, the effective emission rate coefficient of the dielectronic satellite line C_S^{eff}(photons cm^3/s) is obtained as follows (see, for example, [3,23])

$$C_S^{eff}(i,\ j) = 3.3 \times 10^{-24} \left(\frac{I_H}{k_B T_e}\right)^{3/2} \widetilde{Q}_d(i,\ j) exp\left(-\frac{E_S(i)}{k_B T_e}\right) \tag{3}$$

where I_H is the ionization potential of hydrogen, $E_S(i)$ is the energy of the autoionizing state *i,* and T_e is the electron temperature. Atomic data for the KK hollow He-like F ions involved in Eqs. (2 and 3) were calculated using the MZ approach based on perturbation theory Z expansion [4–7] and are compared well with the most recent results in Ref. [8].

Fig. 2 displays DS spectra ($2lnl' \rightarrow 1snl''$, n = 2,3,4, and 5) from He-like F^{7+} ions calculated using Eq. (3) at electron temperature T_e = 400 eV. After the C_S^{eff} is calculated, a Gaussian broadening is applied. The resolution is arbitrarily chosen such that the individual transitions are not blending and held constant for every line. The values of $E_s(i)$ were between 583 and 608 eV and were assumed having an average value of 600 eV for n = 2 spectra, while were increased for high-Rydberg states to 725 eV, 770 eV, and 790 eV (for n = 3, 4, and 5 spectra, respectively). Commonly used for temperature diagnostics DS lines J ($2p^2\ ^1D_2 \rightarrow 1s2p\ ^1P_1$) at λ=15.286 Å, Q ($2s2p\ ^3P_2 \rightarrow 1s2s\ ^3S_1$) at λ=15.213 Å, R ($2s2p\ ^3P_1 \rightarrow 1s2s\ ^3S_1$) at λ=15.216 Å, T ($2s2p\ ^1P_1 \rightarrow 1s2s\ ^1S_0$) at λ=15.140 Å, and M ($2p^2\ ^1S_0 \rightarrow 1s2p\ ^1P_1$) at λ=15.037 Å are shown in Fig. 2a. For the transitions $2lnl' \rightarrow 1snl''$ with $n > 2$, the strongest lines (with the largest values of $\widetilde{Q}_d$) due to $2pnd\ ^3F_4 \rightarrow 1snd\ ^3D_3$ transitions ($\lambda^{n=3}$ = 15.046 Å, $\lambda^{n=4}$ = 15.011 Å, and $\lambda^{n=5}$ = 14.997 Å) are denoted as 1, 1′, and 1′′ and due to the $2pnd\ ^1F_3 \rightarrow 1snd\ ^1D_2$ transitions ($\lambda^{n=3}$ = 14.959 Å, $\lambda^{n=4}$ = 14.973 Å, and $\lambda^{n=5}$ = 14.978 Å) as 2, 2′, and 2′′, respectively. The next strongest lines labeled 3, 3′, and 3′′ are to $2pnd\ ^3F_3 \rightarrow 1snd\ ^3D_2$ transitions

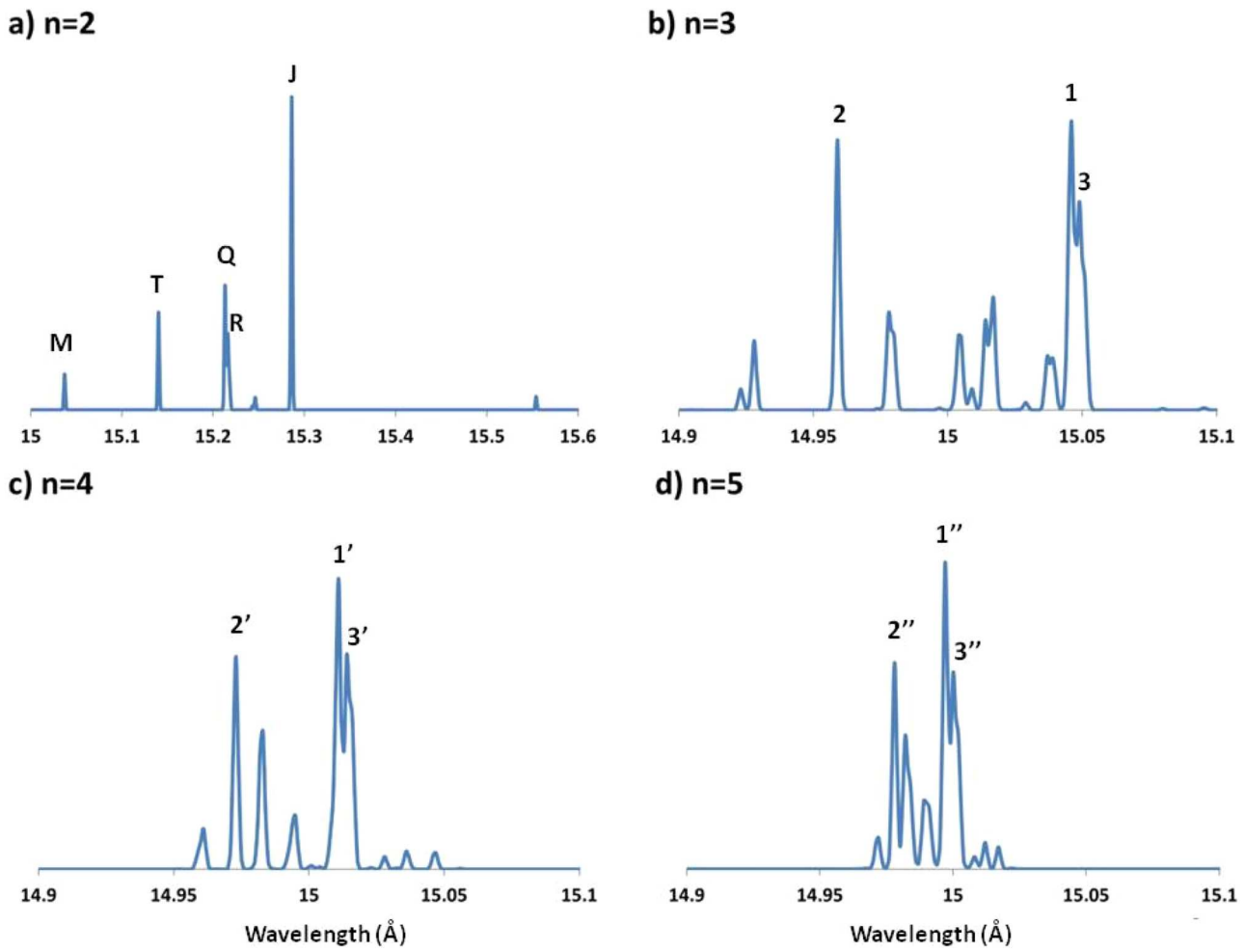

Fig. 2. Dielectronic satellite spectra from doubly-excited states ($2lnl' \rightarrow 1snl''$) from the He-like F ions calculated at $T_e = 400$ eV for $n = 2$ (a), $n = 3$ (b), $n = 4$ (c), and $n = 5$ (d).

for $n = 3$, 4, and 5, respectively. All those lines are satellite lines to the $2p_{3/2}$, $2p_{1/2} \rightarrow 1s_{1/2}$ resonance lines with wavelengths equal to 14.982 Å and 14.988 Å, respectively.

In general, the DR process to the bound state of a Li-like ion involves the capture of an electron by a He- like ion to an autoionizing doubly-excited level of the resulting Li-like ion followed by radiative decay to a singly-excited bound level:

$$\begin{array}{c} F^{7+}(1s^2) + e \rightarrow F^{6+**}(1s2ln'l') \rightarrow F^{7+*}(1s^2 n_1 l_1) + h\nu \\ \downarrow \\ F^{7+}(1s^2) + e \end{array} \quad (4)$$

The ground level of F^{7+}, $1s^2$, is the initial level. The $1s2ln'l'$ levels are taken into account as autoionizing intermediate levels. During the DR process, a DS line is emitted, $h\nu$, when the electron jumps from an autoionizing doubly-excited state to a singly-excited bound state $1s^2nl$. Radiative transitions from the doubly-excited $1s2ln'l'$ states to the $1s^2n_1l_1$ states give rise to commonly used DS lines in He-like F (see Fig. 1). It is a well-known process that was extensively studied both in low- and high-density plasmas for a broad range of Li-like ions and their applications up to $Z = 80$ (see, for example, [25]).

We have calculated DS spectra ($1s2lnl' \rightarrow 1s^2nl''$ with $n = 2$, 3, 4, and 5) for the Li-like F^{6+} ion that occupy the spectral region between 16.8 and 17.2 Å. For $n = 2$, commonly used for temperature DS lines are j ($1s2p^2\ ^2D_{5/2} \rightarrow 1s^22p\ ^2P_{3/2}$) at λ=17.172 Å and k ($1s2p^2\ ^2D_{3/2} \rightarrow 1s^22p\ ^2P_{1/2}$) at λ=17.167 Å. For the transitions $1s2lnl' \rightarrow 1s^2nl''$ with $n > 2$, the strongest lines (with the largest values of $\widetilde{Q}_d$) are due to $1s2pnd\ ^2F_{7/2} \rightarrow 1s^2nd\ ^2D_{5/2}$ transitions ($\lambda^{n=3} = 16.847$ Å, $\lambda^{n=4} = 16.825$ Å, and $\lambda^{n=5} = 16.817$ Å) and due to the $1s2pnp\ ^2D_{5/2} \rightarrow 1s^2np\ ^2P_{3/2}$ transitions ($\lambda^{n=3} = 16.862$ Å, $\lambda^{n=4} = 16.835$ Å, and $\lambda^{n=5} = 16.822$ Å). We did not include and dicuss these DS spectra because they are outside the spectral range of interest of this paper. Also, a critical compilation of experimental data on the $1s2l2l'$ core-excited states of Li-like ions from carbon to uranium discusses the atomic data and their uncertainties for such states in detail in Ref. [26].

In addition, the energy level diagram in Fig. 1 indicates that additional decay channels for the high-Rydberg autoionizing states can occur. For doubly-excited Li-like ion states, the $1s2ln'l'$ states have autoionization decays to $1s^2$ as shown in Eq. (4) but the $1s3l3l'$ states have strong autoionization decays to $1s2l$, which can be larger than to $1s^2$ by a few orders of magnitude. For example, the values of A_a for $1s3d^2$ $J = 7/2$ and 9/2 states can exceed $5 \times 10^{14}\ s^{-1}$, which is 4 orders of magnitude higher than that to $1s^2$.

3. Atomic data and dielectronic satellite spectra from hollow triply-excited states in Li-like fluorine

For the hollow Li-like ions, the DR process involves the capture of an electron by a He-like ion to a hollow triply-excited state of the resulting Li-like ion followed by radiative decay to autoionizing doubly-excited levels. Atomic data (energy levels, radiative transition rates, autoionization decay rates, and intensity factors) for transitions from the hollow $2s^22p$, $2s2p^2$, and $2p^3$ states in Li-like F are listed in Tables 1 and 2. We used the Flexible Atomic Code (FAC) [27] and COWAN code [28] to calculate these atomic data and to compare the results to estimate the

Table 1
Excitation energies counted from the $1s^2 2s\ ^2S_{1/2}$ ground state (E in eV), sums of weighted radiative transition rates ($\sum gA_r$ in 1/s), and total weighted autoionization decay rates (gA_a in 1/s) for the hollow $2s^2 2p$, $2s2p^2$, and $2p^3$ states calculated by COWAN and FAC codes for Li-like F ions. The relative percentage differences between the results of two codes are listed in percentages. A[B] means Ax10^B.

Hollow States	E(eV)		Diff.	$\Sigma\ gA_r\ (s^{-1})$		Diff.	$gA_a\ (s^{-1})$		Diff.
	COWAN	FAC		COWAN	FAC		COWAN	FAC	
$2s^2 2p\ ^2P_{1/2}$	1516.1	1513.9	0.15 %	8.59[12]	7.77[12]	9.5 %	5.07[14]	5.35[14]	−5.5 %
$2s^2 2p\ ^2P_{3/2}$	1516.3	1514.1	0.15 %	1.73[13]	1.56[13]	9.8 %	1.02[15]	1.07[15]	−4.9 %
$2s2p^2\ ^4P_{3/2}$	1516.2	1514.2	0.13 %	2.81[13]	2.55[13]	9.3 %	8.52[13]	6.67[13]	21.7 %
$2s2p^2\ ^4P_{1/2}$	1516.1	1514.2	0.12 %	1.41[13]	1.28[13]	9.2 %	4.26[13]	3.35[13]	21.4 %
$2s2p^2\ ^4P_{5/2}$	1516.3	1514.3	0.13 %	4.22[13]	3.83[13]	9.2 %	1.28[14]	9.94[13]	22.3 %
$2s2p^2\ ^2D_{5/2}$	1526.1	1525.2	0.06 %	3.97[13]	3.64[13]	8.3 %	1.66[15]	1.93[15]	−16.3 %
$2s2p^2\ ^2D_{3/2}$	1526.1	1525.2	0.06 %	2.65[13]	2.43[13]	8.3 %	1.11[15]	1.28[15]	−15.3 %
$2s2p^2\ ^2S_{1/2}$	1532.1	1532.7	0.04 %	1.48[13]	1.30[13]	12.2 %	3.18[14]	3.44[14]	−8.2 %
$2s2p^2\ ^2P_{1/2}$	1533.7	1533.8	−0.01 %	1.41[13]	1.26[13]	10.6 %	3.39[14]	3.48[14]	−2.7 %
$2s2p^2\ ^2P_{3/2}$	1533.8	1533.9	−0.01 %	2.82[13]	2.53[13]	10.3 %	6.79[14]	6.94[14]	−2.2 %
$2p^3\ ^2D_{5/2}$	1536.6	1535.9	0.05 %	5.97[13]	5.41[13]	9.4 %	1.79[15]	2.18[15]	−21.8 %
$2p^3\ ^2D_{3/2}$	1536.6	1536.1	0.03 %	3.98[13]	3.61[13]	9.3 %	1.19[15]	1.45[15]	−21.8 %
$2p^3\ ^2P_{1/2}$	1543.4	1544.2	−0.05 %	1.94[13]	1.72[13]	11.3 %	3.38[14]	2.98[14]	−17.8 %
$2p^3\ ^2P_{3/2}$	1543.4	1544.4	−0.06 %	3.88[13]	3.44[13]	11.3 %	6.74[14]	7.95[14]	−18.0 %

Table 2
Wavelengths (λ in Å), intensity factors ($\widetilde{Q}_d$ in 1/s), and radiative transition rates (gA_r in 1/s) between the upper hollow $2s^2 2p$, $2s2p^2$, and $2p^3$ states and lower autoionizing $1s2s^2$, $1s2s2p$, and $1s2p^2$ states in Li-like F ions calculated using COWAN and FAC codes. The relative percentage differences in radiative transition rates between two codes are listed in percentages. A[B] means Ax10^B.

Line label	Hollow Upper states	Autoionizing Lower states	λ (Å)	$\widetilde{Q}_d$ (s^{-1})	A_r (s^{-1})	A_r (s^{-1})	Diff.
			COWAN			FAC	
Li10	$2s2p^2\ ^2S_{1/2}$	$1s2s2p\ ^2P_{a1/2}$	15.343	4.60[12]	2.38[12]	2.00[12]	16.0 %
Li10	$2s2p^2\ ^2S_{1/2}$	$1s2s2p\ ^2P_{a3/2}$	15.345	8.28[12]	4.28[12]	3.66[12]	17.1 %
Li7	$2p^3\ ^2P_{3/2}$	$1s2p^2\ ^2D_{5/2}$	15.360	9.23[12]	2.39[12]	2.09[12]	12.5 %
Li7	$2p^3\ ^2P_{1/2}$	$1s2p^2\ ^2D_{3/2}$	15.361	5.72[12]	2.96[12]	2.55[12]	13.8 %
Li6	$2p^3\ ^2P_{3/2}$	$1s2p^2\ ^2P_{1/2}$	15.382	2.76[12]	7.14[11]	6.28[11]	12.0 %
Li6	$2p^3\ ^2P_{1/2}$	$1s2p^2\ ^2P_{1/2}$	15.383	5.83[12]	3.02[12]	2.68[12]	11.3 %
Li6	$2p^3\ ^2P_{3/2}$	$1s2p^2\ ^2P_{3/2}$	15.384	1.57[13]	4.06[12]	3.54[12]	12.6 %
Li6	$2p^3\ ^2P_{1/2}$	$1s2p^2\ ^2P_{3/2}$	15.385	2.52[12]	1.31[12]	1.17[12]	10.7 %
Li8a	$2s^2 2p\ ^2P_{3/2}$	$1s2s^2\ ^2S_{1/2}$	15.397	1.33[13]	3.37[12]	3.05[12]	9.5 %
Li8b	$2s^2 2p\ ^2P_{1/2}$	$1s2s^2\ ^2S_{1/2}$	15.402	6.64[12]	3.37[12]	3.04[12]	9.8 %
Li5a	$2s2p^2\ ^2P_{3/2}$	$1s2s2p\ ^2P_{b1/2}$	15.416	4.11[12]	1.07[12]	9.30[11]	13.1 %
Li5a	$2s2p^2\ ^2P_{3/2}$	$1s2s2p\ ^2P_{b3/2}$	15.416	2.03[13]	5.31[12]	4.55[12]	14.3 %
Li5b	$2s2p^2\ ^2P_{1/2}$	$1s2s2p\ ^2P_{b3/2}$	15.419	3.73[12]	1.95[12]	1.66[12]	14.9 %
Li5b	$2s2p^2\ ^2P_{1/2}$	$1s2s2p\ ^2P_{b1/2}$	15.419	8.34[12]	4.36[12]	3.75[12]	14.0 %
Li2	$2s2p^2\ ^2D_{3/2}$	$1s2s2p\ ^2P_{a1/2}$	15.459	1.96[13]	4.97[12]	4.35[12]	12.5 %
Li2	$2s2p^2\ ^2D_{5/2}$	$1s2s2p\ ^2P_{a3/2}$	15.460	3.56[13]	6.02[12]	5.26[12]	12.5 %
Li2	$2s2p^2\ ^2D_{3/2}$	$1s2s2p\ ^2P_{a3/2}$	15.460	3.87[12]	9.83[11]	8.52[11]	13.3 %
Li3a	$2s2p^2\ ^4P_{5/2}$	$1s2s2p\ ^4P_{3/2}$	15.467	1.18[13]	2.11[12]	1.91[12]	9.5 %
Li3a	$2s2p^2\ ^4P_{3/2}$	$1s2s2p\ ^4P_{1/2}$	15.468	1.10[13]	2.93[12]	2.65[12]	9.6 %
Li3a	$2s2p^2\ ^4P_{5/2}$	$1s2s2p\ ^4P_{5/2}$	15.469	3.75[12]	4.92[12]	4.45[12]	9.4 %
Li3a	$2s2p^2\ ^4P_{3/2}$	$1s2s2p\ ^4P_{3/2}$	15.469	2.76[13]	9.35[11]	8.49[11]	9.2 %
Li3b	$2s2p^2\ ^4P_{1/2}$	$1s2s2p\ ^4P_{3/2}$	15.471	1.09[13]	5.86[12]	5.31[12]	9.4 %
Li3b	$2s2p^2\ ^4P_{3/2}$	$1s2s2p\ ^4P_{5/2}$	15.471	1.18[13]	3.16[12]	2.86[12]	9.5 %
Li1	$2p^3\ ^2D_{5/2}$	$1s2p^2\ ^2D_{5/2}$	15.491	1.70[13]	4.78[12]	4.30[12]	10.0 %
Li1	$2p^3\ ^2D_{3/2}$	$1s2p^2\ ^2D_{3/2}$	15.491	2.81[13]	4.33[12]	3.92[12]	9.5 %
Li1	$2p^3\ ^2D_{3/2}$	$1s2p^2\ ^2D_{5/2}$	15.491	2.98[12]	5.66[11]	4.08[11]	12.0 %
Li4b	$2p^3\ ^2D_{3/2}$	$1s2p^2\ ^2P_{1/2}$	15.514	1.61[13]	4.10[12]	3.72[12]	9.3 %
Li4a	$2p^3\ ^2D_{5/2}$	$1s2p^2\ ^2P_{3/2}$	15.516	2.74[13]	4.65[12]	4.25[12]	8.6 %
Li4a	$2p^3\ ^2D_{3/2}$	$1s2p^2\ ^2P_{3/2}$	15.516	3.71[12]	9.47[11]	8.55[11]	9.7 %
Li9	$2p^3\ ^2P_{3/2}$	$1s2p^2\ ^2S_{1/2}$	15.530	8.83[12]	2.29[12]	2.10[12]	9.0 %
Li9	$2p^3\ ^2P_{1/2}$	$1s2p^2\ ^2S_{1/2}$	15.530	4.50[12]	2.38[12]	2.15[12]	9.7 %

accuracy of calculations. The FAC is a complete software package for computation of various atomic radiative and collisional processes and employs a fully relativistic approach based on the Dirac equation and the continuum orbitals are obtained by solving the Dirac equations with the same central potential as that for bound orbitals [27]. We have recently successfully used FAC atomic data for various plasma applications with mid-Z [29] and high-Z (W) [24] ions. COWAN code uses a quasir-elativistic Hartree-Fock method with superposition of configurations and is based on the famous book of R.D. Cowan (see [28] and also the most recent review paper [30]). It includes a least-squares fitting of atomic energy levels (i.e., adjusting the Slater parameters to fit experimental levels), which provides a capability to produce more accurate transitions rates. However, the expected accuracy of the calculated transition rates is within 20 % for the strongest transitions, due to the limitations of the method [30].

We studied the convergence with respect to the configuration interaction using the FAC. For applications which FAC is primarily designed for, it is typically recommended to include only configurations within the same complex, except for some low-lying configurations. However, we consider it very important to study convergence of atomic data for hollow ions and here investigated convergence of the energy levels, radiative transition rates, and autoionization decays rates for

hollow Li-like F ions. We performed calculations by consistently adding configurations up to $n = 10$ (with orbital momentum $l = 0$–3), which increased the number of levels in the model from 529 ($n = 3$) to 5954 ($n = 10$). Then we studied the dependence of the relative percentage of the results (calculated at neighboring quantum numbers) from values of n. For energies of hollow states, we found that the relative percentage change decreased from $\Delta_{34} = 0.38$ %–0.6 % to $\Delta_{67} = 0.049$ %–0.084 % to $\Delta_{910} = 0.016$ %–0.028 %, with the better convergence (smallest values) for the level $2s2p^2\ ^2S_{1/2}$ (lowest values shown above) and the slower convergence for the levels $2s2p^2\ ^2P_{1/2}$, $^2P_{3/2}$, and $2s2p^2\ ^4P_{1/2}$ (at or close to the highest values shown above). For the sum of radiative transition rates (summed over all radiative decay channels), these numbers changed from $\Delta_{34} = 0.6$ %–1.6 % to $\Delta_{67} = 0.16$ %–0.42 % to $\Delta_{910} = 0.08$ %–0.14 %. The better convergence (smallest values) was observed again for the level $2s2p^2\ ^2S_{1/2}$ (lowest values shown above) and the slower convergence for the levels $2s^22p\ ^2P_{1/2}$, $^2P_{3/2}$, and $2s2p^2\ ^4P_{5/2}$ (at or close to the highest values shown for Δ_{910} above). For autoionization decay rates, the relative percentage change was somewhat higher than for the sum of radiative transition rates, from $\Delta_{34} = 3.2$ %–5.0 % to $\Delta_{67} = 0.43$ %–0.66 % to $\Delta_{910} = 0.13$ %–0.21 %. To illustrate the major tendencies, we included the graph for autoionization decay rates (see Fig. 3). The slower convergence is for three quartet states $2s2p^2\ ^4P_{1/2}$, $^4P_{3/2}$, and $^4P_{5/2}$ (at or close to the highest values shown above), which is illustrated by dark red trace in Fig. 3 (which is an overlap of three traces).

Table 1 lists excitation energies (counted from the $1s^22\ s\ ^2S_{1/2}$ ground state in eV), sums of weighted radiative transition rates ($\sum gA_r$ in 1/s), and total weighted autoionization decay rates (gA_a in 1/s) for the hollow $2s^22p$, $2s2p^2$, and $2p^3$ states calculated by COWAN and FAC codes for Li-like F and the comparison of the results from these two codes. The relative percentage difference for the atomic data (difference between the COWAN and FAC results divided by the COWAN result) is listed in columns named "Diff.". For excitation energies, such a difference is very small (≤ 0.15 %) with the best agreement (in absolute values) for the hollow states $2s2p^2\ ^2P_{1/2,3/2}$ (0.01 %), $2p^3\ ^2D_{3/2}$ (0.03 %), $2s2p^2\ ^2S_{1/2}$ (0.04 %), and $2p^3\ ^2P_{1/2,}\ ^2D_{5/2}$ (0.05 %). For the sum of weighted radiative transition rates, this difference is larger, which was expected but with a smaller dispersion, from 8.3 % for the hollow states $2s2p^2\ ^2D_{3/2,5/2}$ to 11.3 % for the hollow states $2p^3\ ^2P_{1/2}$, $^2P_{3/2}$. Lastly, for the total weighted autoionization decays, the absolute values of differences are even larger than those for radiative transition rates with a larger dispersion and changes from as small as 2.2 %–2.7 % for the $2s2p^2\ ^2P_{1/2,3/2}$ to the larger values for the $2s2p^2\ ^4P_{5/2,3/2,1/2}$ (21.4 %–22.3 %) and $2p^3\ ^2D_{3/2,5/2}$ (21.8 %).

Table 2 shows the spectroscopic line labels, hollow upper and autoionizing lower states of radiative transitions in the first three columns, then wavelengths, intensity factors, and radiative transition rates from COWAN code, radiative transition rates from FAC, as well as the comparison of radiative transition rates between these two codes in the last column "Diff." The relative percentage differences changes with a little bit larger dispersion that for the sum of the weighted radiative transition rates but with a smaller than for the total weighted autoionization decay rates in Table 1. The smallest relative percentage difference is for the transition $2p^3\ ^2D_{5/2} \rightarrow 1s2p^2\ ^2P_{3/2}$ (8.6 %). The maximum percentage difference is for transitions $2s2p^2\ ^2S_{1/2} \rightarrow 1s2s2p\ ^2P_{a1/2,a3/2}$ (16.0–17.1 %), which exceeds the largest value for the differences in the sum of radiative transition rates from Table 1 but still within the expected accuracy of FAC radiative transition rates (10–20 %).

There are more autoionization decay channels for hollow triply-excited Li-like ions compared to doubly-excited Li-like states. To demonstrate this important point, Table 3 lists the total autoionization decay rates and contributions of different decay channels (in percentages) for the hollow $2l2l'2l''$ states in Li-like F calculated by the FAC code. The major autoionization decay channels are $1s2s$ and $1s2p$, and autoionization decays to the $1s^2$ is 4–5 orders of magnitude less and to $1s3l$<1 % (not shown in the table). The dominant contributions from most hollow states into the total A_a rates are to the $1s2p\ ^3P_2$ channel with the largest from $2s2p^2\ ^4P_{5/2}$ (73.8 %) and from $2s2p^2\ ^4P_{1/2}$ to the $1s2p\ ^3P_1$ (76.1 %) as well as from $2s2p^2\ ^2D_{5/2,3/2}$ and $^2S_{1/2}$ to the $1s2p\ ^3S_1$ (57.9 % and 43.6 %, respectively). It is more illustrative to discuss in another coupling scheme. Using the *LS* coupling there are four decay channels ($1s2s\ ^3S$, $1s2s\ ^1S$, $1s2p\ ^3P$, and $1s2p\ ^1P$). We can see from Table 3 that hollow Li-like F states autoionize to the following channels: $2s^22p\ ^2P$ to the four channels; $2s2p^2\ ^2D$ and $2s2p^2\ ^2S$ to three channels (^3S, ^1S, ^3P); $2p^3\ ^4S$, $2s2p^2\ ^2P$, $2p^3\ ^2D$, and $2p^3\ ^2P$ to two channels (^3P and ^1P), and $2s2p^2\ ^4P$ to a single channel (^3P). We have learned and discussed in this section how consistently adding configurations up to $n = 10$ will improve the values of autoionization decays also listed in this Table, but it almost did not affect the distribution of percentage contributions among the different channels.

Fig. 4 displays the DS spectrum from hollow Li-like F ions calculated using Eq. (3) and the following parameters: $T_e = 400$ eV and $E_s = 600$ eV. After the C_S^{eff} is calculated, a Gaussian broadening is applied. The resolution is arbitrarily chosen such that the individual transitions are not blending and held constant for every line. Fig. 4a presents the DS spectrum from hollow Li-like F ions in a spectral range 15.35 – 15.55 Å. It includes spectral features Li1 – Li10 specified in Table 1. Specifically, three lines ($2p^3\ ^2D_J \rightarrow 1s2p^2\ ^2D_{J'}$) contribute into Li1 with the most intense line at 15.491 Å ($J = 5/2 \rightarrow J' = 5/2$, $\widetilde{Q}_d = 2.81\times10^{13}\ s^{-1}$); three

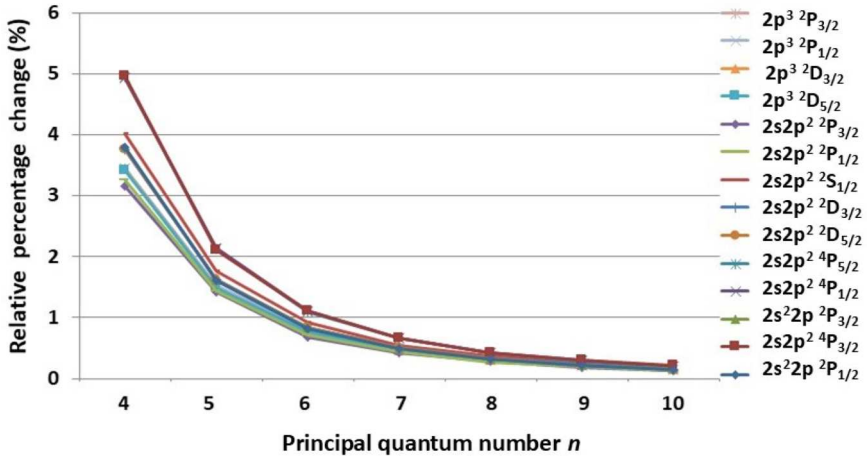

Fig. 3. Relative percentage change of autoionization decay rates from hollow Li-like F ion states calculated using the FAC code as a function of the principal quantum numbers included in the atomic model.

Table 3
The total autoionization decay rates and contributions from different decay channels (in percentages) for the hollow $2l2l'2l''$ states in Li-like F ions calculated by the FAC code.

Hollow states	A_a	1s2s		1s2p			
	(s^{-1})	$^3S_1$	$^1S_0$	$^3P_0$	$^3P_1$	$^3P_2$	$^1P_1$
$2s^22p$ $^2P_{1/2}$	2.68 [14]	8.5 %	15.8 %	16.7 %	35.3 %	5.6 %	18.1 %
$2s^22p$ $^2P_{3/2}$	2.67 [14]	8.5 %	15.5 %	1.2 %	10.9 %	44.7 %	19.2 %
$2s2p^2$ $^4P_{3/2}$	1.67 [13]	0.0	0.0	27.9 %	23.9 %	48.2 %	0.0
$2s2p^2$ $^4P_{1/2}$	1.67 [13]	0.0	0.0	11.3 %	76.1 %	12.6 %	0.0
$2s2p^2$ $^4P_{5/2}$	1.66 [13]	0.0	0.0	0.0	26.2 %	73.8 %	0.0
$2s2p^2$ $^2D_{5/2}$	3.21 [14]	57.9 %	19.3 %	0.0	3.6 %	18.8 %	0.0
$2s2p^2$ $^2D_{3/2}$	3.21 [14]	58.0 %	19.4 %	6.3 %	13.3 %	2.8 %	0.0
$2s2p^2$ $^2S_{1/2}$	1.72 [14]	43.6 %	14.4 %	5.4 %	15.1 %	20.5 %	0.0
$2s2p^2$ $^2P_{1/2}$	1.74 [14]	0.0	0.0	13.2 %	30.7 %	19.6 %	36.5 %
$2s2p^2$ $^2P_{3/2}$	1.73 [14]	0.0	0.0	3.3 %	15.2 %	44.2 %	37.4 %
$2p^3$ $^2D_{5/2}$	3.64 [14]	0.0	0.0	5.5 %	20.6 %	48.7 %	25.2 %
$2p^3$ $^2D_{3/2}$	3.63 [14]	0.0	0.0	12.8 %	32.1 %	30.3 %	24.7 %
$2p^3$ $^2P_{1/2}$	1.99 [14]	1.3 %	2.2 %	2.1 %	14.7 %	54.5 %	25.3 %
$2p^3$ $^2P_{3/2}$	1.99 [14]	1.3 %	2.1 %	10.3 %	27.6 %	34.1 %	24.6 %

lines ($2s2p^2\ ^2D_J \rightarrow 1s2s2p\ ^2P_{J'}$) contribute into Li2 with the most intense line at 15.460 Å ($J = 5/2 \rightarrow J' = 3/2$, $\widetilde{Q}_d = 3.56\times10^{13}\ s^{-1}$); six lines ($2s2p^2\ ^4P_J \rightarrow 1s2s2p\ ^4P_{J'}$) contribute into Li3 with the most intense line at 15.469 Å ($J = 5/2 \rightarrow J' = 5/2$, $\widetilde{Q}_d = 2.76\times10^{13}\ s^{-1}$); three lines ($2p^3\ ^2D_J \rightarrow 1s2p^2\ ^2P_{J'}$) contribute into Li4 with the most intense line at 15.516 Å ($J = 5/2 \rightarrow J' = 3/2$, $\widetilde{Q}_d = 2.74\times10^{13}\ s^{-1}$); four lines ($2s2p^2\ ^2P_J \rightarrow 1s2s2p\ ^2P_{J'}$) contribute into Li5 with the most intense line at 15.416 Å ($J = 3/2 \rightarrow J' = 3/2$, $\widetilde{Q}_d = 2.03\times10^{13}\ s^{-1}$); four lines ($2p^3\ ^2P_J \rightarrow 1s2p^2\ ^2P_{J'}$) contribute into Li6 with the most intense line at 15.384 Å ($J = 3/2 \rightarrow J' = 3/2$, $\widetilde{Q}_d = 1.57\times10^{13}\ s^{-1}$); two lines ($2p^3\ ^2P_J \rightarrow 1s2p^2\ ^2D_{J'}$) contribute into Li7 with the most intense line at 15.360 Å ($J = 3/2 \rightarrow J' = 5/2$, $\widetilde{Q}_d = 9.23\times10^{12}\ s^{-1}$); two lines ($2s^22p\ ^2P_J \rightarrow 1s2s^2\ ^2S_{J'}$) contribute into Li8 with the most intense line at 15.397 Å ($J = 3/2 \rightarrow J' = 1/2$, $\widetilde{Q}_d = 1.33\times10^{13}\ s^{-1}$); two lines ($2p^3\ ^2P_J \rightarrow 1s2p^2\ ^2S_{J'}$) contribute into Li9 with the most intense line at 15.530 Å ($J = 3/2 \rightarrow J' = 1/2$, $\widetilde{Q}_d = 8.83\times10^{12}\ s^{-1}$), and two lines ($2s2p^2\ ^2S_J \rightarrow 1s2s2p\ ^2P_{J'}$) contribute into Li10 with the most intense line at 15.345 Å ($J = 1/2 \rightarrow J' = 3/2$, $\widetilde{Q}_d = 8.28\times10^{12}\ s^{-1}$). The same spectrum is shown in a broader spectral range, which includes Lyα and Heα resonance lines of F ions at λ=14.982 Å and λ=16.809 Å, respectively.

4. Discussion

Jacobs et al. studied the effects of initial-state population variations on the 2p →1 s Kα dielectronic satellite spectra of highly ionized iron ions in high-temperature astrophysical and laboratory plasmas [31]. The authors showed that in addition to the variation in electron temperature (a very important application of dielectronic satellites to plasma diagnostics), which is attributable to the temperature dependences of the radiationless electron capture and inner-shell-electron collisional excitation rate coefficients and to the temperature dependence of the charge-state distribution, the K-shell emission spectra exhibit an electron-density sensitivity [31]. This electron-density sensitivity was suggested to be a result of the density-dependent distribution of populations among the different fine-structure levels of the initial ions in the dielectronic recombination and inner-shell electron collisional excitation processes and a simplified treatment was introduced for the initial distribution of populations, whose precise determination would involve the detailed and self-consistent description of a variety of atomic autoionization, collision, and radiative processes. The electron-density range of interest was subdivided into three, increasingly dense regions with the most dense region characterized by laser-produced and vacuum-spark-produced plasmas [31].

In the present paper, we are interested in the high-energy-density (HED) plasma with electron densities $10^{19}\ cm^{-3} \leq Ne \leq 10^{23}\ cm^{-3}$ which was motivated by our possible observation of the hollow fluorine ions in high-contrast laser-produced plasma experiments with CF_2 targets on Leopard laser facility at UNR [22]. Based on the atomic data calculated and discussed above, we created an atomic model for fluorine ions and used it for non-Local Thermodynamic Equilibrium (non-LTE) modeling with the SUNR code, where energy levels are coupled by collisional excitation and radiative decay and their reverse processes within each ion and by collisional ionization, Auger decay, and photoionization and their reverse processes (three-body, dielectronic, and radiative recombination) in neighboring ions [32,33]. The configurations included in the atomic model are shown in Fig. 1 and comprise 18 H-like, 29 He-like, and 52 Li-like configurations. However, the spectral signatures of hollow Li-like F ions were not intense enough to manifest in the spectral range between the intense Heα and Lyα resonance lines, calculated in the broad ranges of electron density ($N_e = 10^{17}$ - $10^{23}\ cm^{-3}$) and electron temperatures (T_e =100–500 eV). It was confirmed by very low resulting populations of hollow Li-like F ion states, even with inclusion of inner-shell excitation. The analysis of the populations of He-like F ions calculated at T_e =400 eV reveals that all populations of 1s2l levels are almost proportional to their statistical weights in this electron density region with the exception for the level 1s2p $^1P_1$ that needs a higher density ($N_e \geq 10^{22}\ cm^{-3}$). Because a majority of the 1s2l levels, which represent the most important autoionization decay channels for hollow Li-like F ions shown in Table 3, are statistically populated in the range of the electron density of interest, it is justifiable to use the modified intensity factor which includes the sum over all these levels in Eq. (2) as well as the effective emission rate coefficients in Eq. (3) to produce synthetic dielectronic satellite spectra in Fig. 3 (see also [7,31]). Summarizing, (i) the dielectronic satellite spectra of hollow He-like F ions in Fig. 2 are almost not sensitive to the electron density because of only one major channel of the autoionization decay (1s); (ii) the dielectronic spectra of hollow Li-like F ions in Fig. 3 are produced by taking into account all channels of autoionization decays following Eqs. (2 and 3) and atomic data discussed above, as well as statistical distribution of 1s2l levels (which was analyzed using the full non-LTE kinetic modeling), and (iii) these spectra are applicable to the high-density laser-produced plasmas (such as from Leopard laser facility) or Z-pinch plasmas from university scale pulsed-power generator.

5. Conclusion

We have completed the theoretical study of dielectronic satellite lines from hollow He- and Li-like F ion states motivated by current research on hollow ions in HED plasmas and by the results of our previous high contrast laser-produced plasma experiments with CF_2 targets on Leopard laser facility at UNR.

For the hollow Li-like ions, the DR process to a bound state of a Li-like ion involves the capture of an electron by a He-like ion to a hollow triply-excited state of the resulting Li-like ion (for example, $2l2l'2l''$ states) followed by radiative decay to an autoionizing doubly-excited level (for example,$1s2l_12l_2$ states). The accuracy of the atomic data for $1s2l_12l_2$ states were studied in detail before, but not of the atomic data for the KK hollow Li-like states. To address this issue, we studied the convergence with respect to the configuration interaction using the FAC

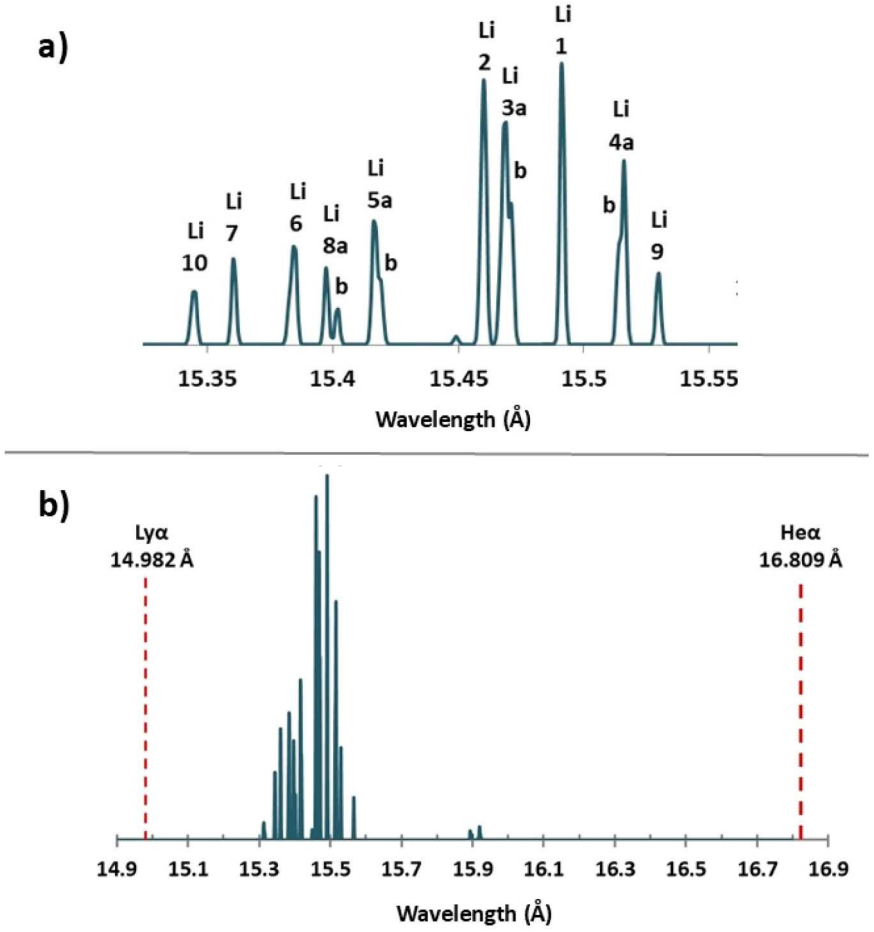

Fig. 4. Theoretical spectra of dielectronic satellite lines from the hollow triply-excited states of Li-like F ions calculated at $T_e = 400$ eV shown: a) in a spectral region 15.35 to 15.55 Å and (b) within a broader spectral region between Lyα and Heα resonance lines of F ions.

and in addition compared the results of COWAN and FAC codes. We performed FAC calculations by consistently adding configurations up to $n = 10$ (with orbital momentum $l = 0$–3), which increased the number of levels in the atomic model from 529 ($n = 3$) to 5954 ($n = 10$). Then we studied the dependence of the relative percentage change of the results as a function of n. For energies of hollow states, we found that the relative percentage change decreased from $\Delta_{34} = 0.38$ %−0.6 % to $\Delta_{910} = 0.016$ %−0.028 %. For the sum of radiative transition rates, these numbers slightly increased to $\Delta_{34} = 0.6$ % −1.6 % and $\Delta_{910} = 0.08$ %−0.14 %, respectively. For autoionization decay rates, the relative percentage changes were somewhat higher than those for the sum of radiative transition rates, but still were decreasing from $\Delta_{34} = 3.2$ %−5.0 % to $\Delta_{910} = 0.13$ %−0.21 % with a slower convergence for three quartet $2s2p^2\ ^4P_{1/2}$, $^4P_{3/2}$, and $^4P_{5/2}$ and two doublet $2p^3\ ^2D_J$ hollow states.

The relative percentage differences for the hollow ion atomic data calculated using COWAN and FAC codes were very small for excitation energies (≤ 0.15 %) with the best agreement (in absolute values) for the hollow states $2s2p^2\ ^2P_{1/2,3/2}$ (0.01 %), $2p^3\ ^2D_{3/2}$ (0.03 %), $2s2p^2\ ^2S_{1/2}$ (0.04 %), and $2p^3\ ^2P_{1/2}$, $^2D_{5/2}$ (0.05 %). For the sum of radiative transitions rates, this differences were larger, which was expected, from 8.3 % for the hollow states $2s2p^2\ ^2D_{3/2,5/2}$ to 11–12 % for the hollow states $2p^3\ ^2P_{1/2,}\ ^2P_{3/2}$, and $2s2p^2\ ^2S_{1/2}$, which is within 10–20 % (typical accuracy for FAC radiative transition calculations). Lastly, for the total autoionization decay rates, the absolute values of differences were even larger than those for radiative transition rates with a larger dispersion and varied from as small as 2.2 %−2.7 % for the doublet $2s2p^2\ ^2P_{1/2,3/2}$ to the larger values, again for the three quartet $2s2p^2\ ^4P_{5/2,3/2,1/2}$ (21.4 %−22.3 %) and for the doublet $2s2p^2\ ^2D_{3/2,5/2}$ (21.8 %) hollow states. However, if the accuracy of radiative transition rates has been studied for some specific types of transitions in detail during the last decade, then there is much less data available on accuracy of the autoionization decay rates, which are more challenging to calculate. We consider our atomic data calculated using the FAC with the atomic model which includes configurations up to $n = 10$ as the most accurate compared to the initial FAC calculations (which included configurations up to $n = 3$) and to COWAN data without experimental data available.

In addition, we found that there are more autoionization decay channels for hollow triply-excited *2l2l'2l''* states compared to doubly-excited *1s2l'2l''* states in Li-like ions. The largest values of A_a rates are for D states ($^2D_{5/2}$ and $^2D_{3/2}$) for both $2p^3$ and $2s2p^2$ hollow configurations. The major autoionization channels are $1s2s$ and $1s2p$ and autoionization decays to the $1s^2$ being 4–5 orders of magnitude less. Using the *LS* coupling there are four decay channels ($1s2s\ ^3S$, $1s2s\ ^1S$, $1s2p\ ^3P$, and $1s2p\ ^1P$) and hollow Li-like F states autoionize to the following channels: $2s^22p\ ^2P$ to the four channels; $2s2p^2\ ^2D$ and $2s2p^2\ ^2S$ to three channels (^3S, ^1S, ^3P); $2p^3\ ^4S$, $2s2p^2\ ^2P$, $2p^3\ ^2D$, and $2p^3\ ^2P$ to two channels (^3P and ^1P), and $2s2p^2\ ^4P$ to a single channel (^3P). Then, if the excited He-like states are populated more in dense plasmas (compared to the moderate- and low-density plasmas) then the satellite lines from hollow ions can have observable line intensities.

For KK hollow Li-like F ions, dielectronic satellite (hypersatellite) lines (*2l2l'2l''*→*1s2l2l'*) cover the spectral region 15.35 to 15.55 Å, which occupies a relatively small portion of a spectral region between Lyα (at 14.982 Å) and Heα (at 16.809 Å) resonance lines of He-like F ions whereas the commonly used satellite lines ($1s2lnl' \rightarrow 1s^2nl''$ with $n = 2$, 3, 4, and 5) cover the spectral range 16.8 – 17.2 Å, which is mostly to the

right of Heα line. The most intense dielectronic satellite lines from hollow Li-like F ions were identified and illustrated in this paper.

The next step will be studying dielectronic satellites from KK hollow Be-like F ion states that our calculations show to occupy the spectral region between 15.6 and 15.8 Å and to have even more addition channels of autoionization decays than hollow Li-like F ion states. Also, we will be including the transitions from autoionizing $1s2l2l'3l'' \rightarrow 1s^2 2l2l'$ states that may partially overlap with the spectral region considered in this paper. In addition, we will work more on detailed comparison of dielectronic satellite spectra of hollow Li- and Be-like F ions (with and without inner-shell collisions) with experimental data to better understand production mechanism of hollow ions in HED plasmas.

CRediT authorship contribution statement

A.S. Safronova: Writing – original draft, Validation, Project administration, Methodology, Investigation, Conceptualization. **A. Stafford:** Writing – review & editing, Formal analysis. **U.I. Safronova:** Validation, Software, Formal analysis.

Declaration of competing interest

The authors declare that they have no known competing financial interests or personal relationships that could have appeared to influence the work reported in this paper.

Acknowledgments

This research was supported by the National Science Foundation and the National Nuclear Security Administration under NSF award PHY-2205769.

Data availability

Data will be made available on request.

References

[1] Gabriel AH, Jordan C. Long wavelength satellites to the He-like resonance lines in the laboratory and in the Sun. Nature 1969;221:947.
[2] Gabriel AH. Dielectronic satellite spectra for highly charged helium-like ion lines. Mon Not R Astr Soc 1972;160:99.
[3] Dubau J, Volonte S. Dielectronic recombination and its applications in astronomy. Rep Prog Phys 1980;43:199.
[4] Vainstein LA, Safronova UI. Wavelengths and transition probabilities of satellites to resonance lines of H- and He-like Ions". At Data Nucl Data Tables 1978;21:49.
[5] Safronova UI, Urnov AM. Perturbation theory Z expansion for many-electron autoionising states of atomic systems. I. Calculations of the energy. J Phys B: Atom Mol Phys 1979;12:3171.
[6] Safronova UI, Urnov AM. Perturbation theory Z expansion for many-electron autoionisation states of atomic system. II. Autoionisation rates and radiative transition probabilities. J Phys B: Atom Mol Phys 1980;13:869.
[7] Safronova UI, Shlyaptseva AS, Urnov AM. Perturbation theory Z-expansion method for autoionisation states of many-electron atomic systems. III. Dielectronic satellite spectra for highly charged ions in a hot dense plasma. J Phys B: Atom Mol Phys 1981;14:1249.
[8] Goryaev FF, Vainshtein LA, Urnov AM. Atomic data for doubly-excited states 2lnl′ of He-like ions and 1s2lnl′of Li-like ions with Z = 6–36 and n = 2, 3. At Data Nucl Data Tables 2017;113:117.
[9] Safronova UI, Senashenko VS. The radiative decay of excited states of atomic systems with two K-shell vacancies. J Phys B: At Mol Opt Phys 1977;10:L271.
[10] Safronova UI, Senashenko VS. Autoionising states of three-electron atomic systems. J Phys B 1978;11:2623.
[11] Bruch R, Paul G, Andra J, Lipsky L. Autoionization of foil-excited states in Li I and Li II. Phys Rev A 1975;12:1808.
[12] Safronova UI, Bruch R. Triply Excited States of the Lithium Isoelectronic Sequence: Z=3-54. Phys Scr 1998;57:519.
[13] Faenov AYa, Magunov AI, Pikuz TA, Skobelev IYu, Pikuz SA, Urnov AM, Abdallah J, Clark REH, Cohen J, Johnson RP, Kyrala GA, Wilke MD, Maksimchuk A, Umstadter D, Nantel N, Doron R, Behar E, Mandelbaum P, Schwob JJ, Dubau J, Rosmej FB, Osterheld AL. High-resolved X-ray spectra of hollow atoms in a femtosecond laser-produced solid plasma. Phys Scr 1999;T80:536.
[14] Skobelev IYu, Faenov AYa, Pikuz TA, Fortov VE. Spectra of hollow ions in an ultradense laser plasma. Phys Usp 2012;55:47.
[15] Faenov AYa, Skobelev IYu, Pikuz TA, Fortov VE, Boldarev AS, Gasilov VA, Chen LM, Zhang L, Yan WC, Yuan DW, Mao JY, Wang ZH, Colgan J, Abdallah Jr J. Diagnostics of the early stage of the heating of clusters by a femtosecond laser pulse from the spectra of hollow ions. JETP Lett 2011;94:171.
[16] Rosmej FB, Faenov AYa, Pikuz TA, Magunov AI, Skobelev IYu, Auguste T, D'Oliveira P, Hulin S, Monot P, Andreev NE, Chegotov MV, Veisman ME. Charge-exchange-induced formation of hollow atoms in high-intensity laser-produced plasmas. J Phys B: At Mol Opt Phys 1999;32:L107.
[17] Rosmej F, Hoffmann DHH, Suess W, Geissel M, Rosmej ON, Faenov AYa, Pikuz T, Auguste T, D'Oliveira P, Hulinc S, et al. High-resolution X-ray imaging spectroscopy diagnostic of hollow ions in dense plasmas. Nucl Instr Methods Phys Res A 2001;464:257.
[18] Rosmej FB, Dachicourt R, Deschaud B, Khaghani D, Dozières M, Šmíd M, Renner O. Exotic x-ray emission from dense plasmas. J Phys B: At Mol Opt Phys 2015;48:224005.
[19] Colgan J, Ḥ J, Faenov AYa, Pikuz SA, Wagenaars E, Booth N, Culfa O, Dance RJ, Evans RG, Gray RJ, Kaempfer T, Lancaster KL, McKenna P, Rossall AL, Skobelev IYu, Schulze KS, Uschmann I, Zhidkov AG, Woolsey NC. Exotic dense-matter states pumped by a relativistic laser plasma in the radiation-dominated regime. Phys Rev Lett 2013;110:125001.
[20] Hansen SB, Colgan J, Faenov AYa, Abdallah J, Pikuz SA, Skobelev IYu, Wagenaars E, Booth N, Culfa O, Dance RJ, Tallents GJ, Evans RG, Gray RJ, Kaempfer T, Lancaster KL, McKenna P, Rossall AK, Schulze KS, Uschmann I, Zhidkov AG, Woolsey NC. Detailed analysis of hollow ions spectra from dense matter pumped by X-ray emission of relativistic laser plasma. Phys Plasmas 2014;21:031213.
[21] Colgan J, Faenov AYa, Pikuz SA, Tubman E, Butler NMH, Abdallah jr J, Dance RJ, Pikuz TA, Skobelev IYu, Alkhimova MA, Booth N, Green J, Gregory C, Andreev A, Lotzsch R, Uschmann I, Zhidkov A, Kodama R, McKenna P, Woolsey N. Evidence of high-n hollow-ion emission from Si ions pumped by ultraintense x-rays from relativistic laser plasma. Europhys Lett 2016;114:35001.
[22] Safronova AS, Kantsyrev VL, Faenov AY, Safronova UI, Wiewior P, Renard-Le Galloudec N, Esaulov AA, Weller ME, Stafford A, Wilcox P, Shrestha I, Ouart ND, Shlyaptseva V, Osborne GC, Chalyy O, Paudel Y. Atomic physics of relativistic high contrast laser-produced plasmas in experiments on Leopard laser facility at UNR. High Energy Density Phys 2012;8:190.
[23] Stafford A, Safronova AS, Safronova UI, Kantsyrev VL, Faenov AY, Wiewior P, Weller ME, Shrestha I, Shlyaptseva VV, Paudel Y. Analysis of Mg spectral features produced by irradiations of laser pulses with different contrast and pulse durations. J Phys B: At Mol Opt Phys 2014;47:065001.
[24] Safronova AS, Stafford A, Gill AK, Childers RR. Polarization of hard X-ray dielectronic satellite line emission from Na-like W ions. J Quant Spectrosc Radiat Transfer 2021;272:107788.
[25] Safronova UI, Safronova AS, Johnson WR. Relativistic many-body calculations of dielectronic satellite spectra created by autoionizing 1s2l2l' states in Li-like ions. J Phys B: At Mol Opt Phys 2010;43:074026.
[26] Azarov VI, Kramida A, Ralchenko Yu. A critical compilation of experimental data on the 1s2l2l′ core-excited states of Li-like ions from carbon to uranium. At Data Nucl Data Tables 2023;149:101548.
[27] Gu MF. The flexible atomic code. Can J Phys 2008;86:675.
[28] Childers RR, Safronova AS, Kantsyrev VL, Stafford A, Gill AK. K-shell radiation and bright spot characteristics of high-energy-density Fe-Cr-Ni plasmas influenced by X-pinch load geometry. J Quant Spectrosc Radiat Transf 2023;303:108586.
[29] Cowan RD. The theory of atomic structure and spectra. Berkeley: University of California Press; 1981.
[30] Kramida A. Cowan code: 50 years of growing impact on atomic physics. Atoms 2019;7:64. https://doi.org/10.3390/atoms7030064.
[31] Jacobs VL, Doschek GA, Seely JF, Cowan RD. Effects of initial-state population variations on the 2p →1s Ka dielectronic satellite spectra of highly ionized iron ions in high-temperature astrophysical and laboratory plasmas. Phys Rev A 1989;39:2411.
[32] Hansen S. PhD dissertation, "Development and application of L-shell spectroscopic modeling for plasma diagnostics. Reno: University of Nevada; 2003.
[33] Ouart ND, Safronova AS, Kantsyrev VL, Esaulov AA, Williamson KM, Shrestha I, Osborne GC, Weller ME. Studies of radiative and implosion characteristics from brass planar wire arrays. IEEE Trans Plasma Sci 2010;34(4):631–8.